PAPER • OPEN ACCESS

Promoting rebound of impinging viscoelastic droplets on heated superhydrophobic surfaces

To cite this article: Bin Li *et al* 2020 *New J. Phys.* **22** 123001

View the article online for updates and enhancements.

New Journal of Physics

The open access journal at the forefront of physics

Deutsche Physikalische Gesellschaft **DPG**

IOP Institute of Physics

Published in partnership with: Deutsche Physikalische Gesellschaft and the Institute of Physics

CrossMark

OPEN ACCESS

PAPER

Promoting rebound of impinging viscoelastic droplets on heated superhydrophobic surfaces

Bin Li[1,2], Shiji Lin[1], Yile Wang[1], Quanzi Yuan[3,4], Sang W Joo[2,*] and Longquan Chen[1,*]

1 School of Physics, University of Electronic Science and Technology of China, Chengdu 610054, People's Republic of China
2 School of Mechanical Engineering, Yeungnam University, Gyeongsan 38541, Republic of Korea
3 State Key Laboratory of Nonlinear Mechanics, Institute of Mechanics, Chinese Academy of Sciences, Beijing 100190, People's Republic of China
4 School of Engineering Science, University of Chinese Academy of Sciences, Beijing 100049, People's Republic of China
* Authors to whom any correspondence should be addressed.

E-mail: lqchen@uestc.edu.cn and swjoo@yu.ac.kr

Abstract

The rebound of impinging droplets is a defining characteristic of superhydrophobic surfaces; yet, such an intriguing interfacial phenomenon can be effectively suppressed by adding a tiny amount of flexible polymers to induce non-Newtonian viscoelastic properties. In this work, however, we demonstrate the promoting effects of surface heating on the rebound of impinging viscoelastic droplets on superhydrophobic surfaces. The underlying mechanism for the promotion is that the local heat transfer at the liquid–solid interface causes the fast evaporation of the liquid and thus the breakup of the formed viscoelastic filaments, which hinder droplet recoiling. Therefore, the lower threshold velocity for rebound increases while the upper threshold velocity for rebound suppression decreases with increasing surface temperature, resulting in a wider regime for droplet rebound in the impact phase diagram. The surface heating effect on liquid–solid interactions also leads to a nontrivial dependence of the contact time on the impact velocity and a linear decrease of the restitution coefficient with the Weber number for diverse bouncing viscoelastic droplets, which can be rationalized by coupling the interfacial force and energy analyses. We envision that these findings would be useful in technological processes requiring control the retention of viscoelastic liquids on solid surfaces.

1. Introduction

Anti-wetting is an essential ability of biological systems living on the water-covered Earth [1], and various biosurfaces, including plant leaves [2, 3], insect wings [4], and animal feathers [5, 6], were found to be superhydrophobic. Micromorphology investigations revealed that these different biosurfaces have one characteristics in common: they are built of hydrophobic micro-/nanoscale structures, and thus can entrap a thin layer of air to separate the liquid from the solid [7]. As a result, an aqueous droplet beads up with a contact angle higher than 150° on the superhydrophobic surface, referring as the Cassie–Baxter state [8], and a slight inclination of the surface may cause the droplet rolling off [9]. The superhydrophobicity can even be maintained in a dynamic condition—an impinging droplet would rebound off the surface when its kinetic energy is sufficiently high to compensate the energy dissipated during impact, i.e. the impact velocity should be higher than a lower threshold [10, 11]. However, if the velocity exceeds an upper threshold, the separating air film breaks down upon impact, and the impinging droplet eventually sticks on the surface due to the wetting of the microscopic structures [12, 13], i.e. the droplet transits from the Cassie–Baxter state to the well-known Wenzel state [14].

The rebound of impinging droplets is an undesired phenomenon in agricultural spray since it reduces fluid transfer and thereby pesticide deposition [15, 16]. One remarkable strategy to prevent droplet rebound is by adding a tiny amount (down to ~ 0.1 gl^{-1}) of flexible polymers in the fluid [17, 18], which significantly slows down droplet retraction because of a few possible mechanisms under debate. The non-Newtonian extensional viscosity that originates from the orientation and stretching of polymer chains during impact was initially considered by Bergeron *et al* as the predominant factor hindering droplet motion, and hence suppressing the rebound [19]. However, this effect cannot explain the insignificant influence of polymer additives on droplet spreading, where strong extensional viscous dissipation is also expected. Later, Bartolo *et al* revised this mechanism and suggested that the non-Newtonian normal stress, which is induced by the stretching of polymer chains under the shear flow near the moving contact line, should be the main cause of the rebound suppression [20]. The generation of the normal stress can rationalize why there is a strong effect of polymer additives during retraction but not during spreading for impinging droplets on hydrophobic surfaces; yet, it fails to explain the impact behavior of polymer-laden droplets on structured superhydrophobic surfaces, where the normal stress is very small whilst the rebound suppression is still achievable [21, 22]. The negligible effect of the non-Newtonian normal stress on droplet impact dynamics was further confirmed by directly measuring the flow velocity within the impinging droplet, which also suggests that an effective friction arising at the retracting contact line is responsible for the suppression phenomenon [23]. Indeed, this mechanism is supported by the rejuvenated rebound of non-Newtonian droplets via nanoparticle enwrapping [22], and the direct visualization of viscoelastic ligaments as a polymer-laden droplet sweeps a superhydrophobic surface in the retraction stage [24].

Though adding polymer additives can effectively alter the outcomes of impinging droplets on solid surfaces, the maximum spreading radii of polymer-laden viscoelastic droplets are barely changed compared to that of Newtonian droplets [21, 24, 25], which are mainly controlled by the shear viscosity. As pointed out by Louhichi *et al* [26], both shear and non-Newtonian extensional viscous dissipations exist in the complex impact process of polymer-laden droplets on solid surfaces, and the dynamics is dominated by the shear rheology due to the liquid–solid contact. Indeed, the authors demonstrated the essential role of the extensional viscosity on the expansion of the polymer-laden droplets levitated on a liquid nitrogen thin layer and thus the enhancement of the maximum spreading due to the shear thinning behavior [26]. The dominant extensional effect was also identified during the droplet–droplet impact, where viscoelastic droplets exhibit less probability to rebound [27]. Moreover, Pack *et al* recently showed that a large increase of the extensional viscosity can significantly damp the capillary wave propagation during impact and thereby inhibit the droplet–surface contact on soft liquid films [28].

In industrial applications such as spray cooling, water-soluble polymers are normally employed to achieve high heat transfer efficiency [29]. Over the past decades, the influence of polymer additives on the impact dynamics on heated hydrophilic surfaces above the boiling temperature has been extensively investigated and well documented [30–33]. In particular, Bertola reported an increase of the maximum rebound height of aqueous polymer droplets on heated aluminium surfaces in the Leidenfrost regime [34], which might be ascribed to the enhanced storage of the impact kinetic energy as the recoverable elastic energy [35].

In this work, we report the impact dynamics of viscoelastic droplets of aqueous polymer solutions on heated superhydrophobic surfaces below the boiling temperature, which has received less attention so far. We demonstrate that surface heating does not influence droplet spreading but significantly speeds up droplet recoiling, and thus promotes the rebound behaviors of impinging viscoelastic droplets on superhydrophobic surfaces. Whereas the contact time of bouncing droplets was found to increase with surface temperature and show a nontrivial dependence on the impact velocity, a linear correlation between the restitution coefficient and the Weber number was identified. These phenomena can be explained by the reduced droplet–surface interaction as a result of the local heat transfer occurring at the liquid–solid interface, and the corresponding scaling models were proposed based on the interfacial force and energy analyses.

2. Experimental methods

Superhydrophobic surfaces were prepared by spray coating silicon wafers with a thin layer of hydrophobized nanoparticles (Ultra Glaco, Soft 99 Co., Japan), which form loose and porous structures (figure S1 (https://stacks.iop.org/NJP/22/123001/mmedia)) and thus own ultralow surface energy. Since the roughness of the solid surfaces would affect the contact line dynamics below the impinging droplets [36], it is essential to fabricate superhydrophobic surfaces with controlled surface roughness. In this work, our superhydrophobic surfaces were spray coated with Glaco nanoparticles for 3 times, which results in a nanoparticle layer with a thickness of ~ 1.5 μm and a root-mean-square average of the height deviations of $R_q \approx 85$ nm (Contour

GT 3D, Bruker). We prepared viscoelastic solutions by dispersing 4M poly (ethylene oxide) (PEO, average molecular weight $M_w = 4 \times 10^6$ g mol^{-1}, Sigma Aldrich, USA) in pure water (18.4 MΩ cm, Millipore Synergy, Darmstadt, Germany). In order to identify the influence of liquid viscoelasticity on the droplet dynamics, the polymer concentration of the solutions should be sufficiently high [25]. Here we study aqueous PEO solutions with mass concentrations of $c_{PEO} = 0.1$ gl^{-1}, 0.5 gl^{-1}, and 1.0 gl^{-1}, whose extensional relaxation time is of the same order of the timescale of droplet impact $\sim \left(\rho R_0^3 / \gamma \right)^{0.5}$ [28], with ρ, γ, R_0 being the density, surface tension and radius of the impinging droplet respectively. Note that there could be a slight variability in the molecular weight of the PEO during the chemical synthesis and so do the aqueous PEO solutions. These solutions have comparable surface tensions as water, but exhibit non-Newtonian shear-thinning properties (figure S2). The static contact angles of 4 μl droplets of all aqueous PEO solutions on the superhydrophobic surface were measured to be $\sim 150°$, while the contact angle hysteresis (i.e. the difference between the advancing and receding contact angles, $\theta_a - \theta_r$) was found to increase from $\sim 8°$ for 0.1 gl^{-1} PEO solution to $\sim 12°$ for 1.0 gl^{-1} PEO solution (table S1), suggesting an enhancement of droplet–surface interaction by adding polymer chains. In each impact event, a droplet of radius $R_0 \approx 1.0$ mm was released from a blunt needle, accelerated by gravity and eventually struck on the target superhydrophobic surface placing on a hot plate (figure S3). We investigated droplet dynamics at an impact velocity (V_0) of 0.04–0.48 m s^{-1}, in which the complete rebound happens, and the corresponding Weber number (We = $\rho V_0^2 / \gamma$) range is 0.05–7.5. The impact process was recorded by a high-speed camera (Phantom, V2012, USA) at 60 000 fps, and further analyzed using a MATLAB algorithm. All impact tests were performed under atmospheric pressure in the surface temperature range of $T = 25°C$–$95°C$, which is below the boiling point (100°C) and well below the Leidenfrost temperature ($\sim 193°C$) of water [37]. Therefore, the influence of liquid boiling and the Leidenfrost effect on the droplet dynamics can be safely neglected. Moreover, the high repeatability of the experimental results also indicates the negligible role of the slight variability of the molecular weights.

3. Results and discussion

3.1. Rebound regime

The promotion of the rebound of viscoelastic droplets on superhydrophobic surfaces via surface heating can be readily demonstrated by comparing the impact process and phenomena of 0.1 gl^{-1} PEO droplets with the same velocity of $V_0 \approx 0.29$ m s^{-1} at three different surface temperatures ($T = 25°C$, 50°C and 95°C). After contacting the surface at 25°C, the droplet spreads out with a violent capillary wave travelling from its bottom to top, resulting in complex deformations as that of low-viscosity Newtonian droplets [38, 39]. As a consequence, a pancake-like structure with a spire, as shown at ~ 3.3 ms in figure 1(a), is formed at the maximal extension. For low-viscosity Newtonian liquids such as water, the spire subsequently punches deeply into the droplet due to its high velocity [38] and thus a cylindrical air cavity is created at the droplet center [40, 41]. With the recoiling of the droplet, the air cavity would be squeezed in the direction normal to the surface, and it may coalesce with the air film or bubble formed below the impinging droplet upon impact, which eventually suppresses droplet rebound on superhydrophobic-like soft surfaces since the liquid wets the surface [42, 43]. By contrast, if polymer chains are added in water, the downward motion of the spire can be significantly damped by the extensional viscosity near the droplet center, inhibiting droplet–surface contact [28]. In our experiments, this damping effect was also identified on superhydrophobic surfaces and it is more pronounced for impinging droplets with high PEO concentrations as the created air cavity is much shallower than of pure water droplets reported in previous studies [40–43]. Meanwhile, numerous viscoelastic filaments were observed near the contact line of the recoiling droplet (illustrated by green arrows at 9.5 ms in figure 1(a)). These filaments are anchored on the superhydrophobic surface and successively pulled out from the droplet once the liquid detaches (supplemental movie S1) [24]. This can be more clearly inferred from the scanning electronic microscopy (SEM) images of polymer residue after impact in figure 1(d), where numerous PEO nanofibers (denoted by green arrows) are deposited around the impact point. With droplet recoiling, they are further stretched, and eventually break up when their maximum limits are reached. Although the droplet can rebound off from the surface, the residual viscoelastic filaments restrict it to resume the spherical shape and be highly lifted up. The spreading characteristics described above were also observed for impinging PEO droplets on heated superhydrophobic surfaces at 50°C and 95°C, as evidenced by the snapshots in figures 1(b) and (c) and also the temporal evolution of the droplet contact radius (R_c) in figure 1(e). However, distinct droplet behaviors were found in the retraction stage. At any given time the formed viscoelastic filaments around the recoiling droplet are less on a hot surface than that on a cold surface (see 6.7–9.5 ms in figures 1(a)–(c), and supplemental movies S1–S3), and the corresponding retraction process is relatively faster (figure 1(e)).
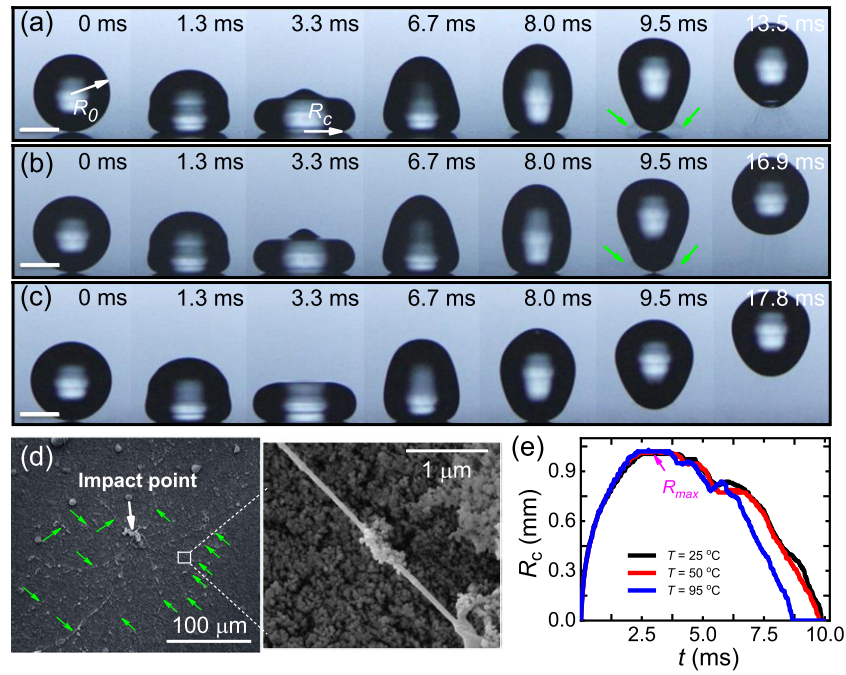
Figure 1. Snapshots of impinging droplets of 0.1 gl^{-1} aqueous PEO solution on superhydrophobic surfaces at 25°C (a), 50°C (b) and 95°C (c). The scale bar is always 1.0 mm. The impact velocity V_0 is ∼0.29 m s^{-1} and the corresponding Weber number We is 2.8. (d) SEM images of residual PEO fibers on the superhydrophobic surface acquired after the impact event in (a). (e) Temporal evolution of the contact radius R_c of impinging droplets in (a)–(c).
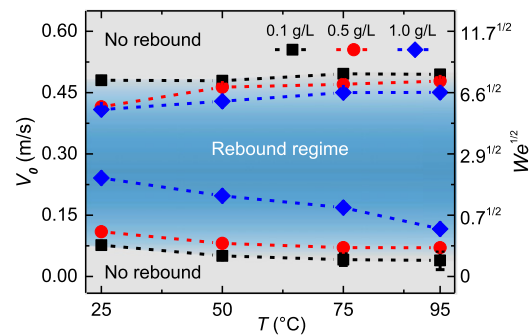
Figure 2. Rebound regimes for viscoelastic droplets of 0.1 gl^{-1}, 0.5 gl^{-1} and 1.0 gl^{-1} aqueous PEO solutions on superhydrophobic surfaces at different temperatures, defined by lower and upper threshold velocities or equivalently the Weber numbers.

Consequently, on a hotter surface the droplet bounces off earlier with a shape comparably more close to a sphere, and the maximum height to which it can reach is relatively higher, particularly on the surface at 95°C (figure 1(c)).

Figure 2 plots the determined lower (V_L) and upper (V_U) threshold velocities of droplet rebound for those three aqueous PEO solutions we investigated. It is seen that the range of the impact velocity or equivalently the Weber number for rebound becomes wider either by increasing surface temperature or by decreasing polymer concentration. More specifically, V_L of all aqueous PEO solutions decreases with increasing T or decreasing c_{PEO}, while V_U shows an increase trend when varying T or c_{PEO} but less obvious.

The nontrivial dependence of the threshold velocities for rebound on the surface temperature and PEO concentration can be understood by an interfacial force analysis. The impact process and outcomes in figures 1(a)–(c) and 1(e) suggest that it is the viscoelastic filaments formed near the contact line leading to a large resistance force, slowing down droplet retraction, and thus determining the thresholds for rebound. Modeling each filament as a simple spring–mass–damper system (i.e. a point mass connected to a purely viscous damper and purely elastic spring in parallel), we derive the resistance force arising from stretching from the equation of motion [44], $f_r = c\dot{L} + kL + m\ddot{L}$. Here L is the length of the filament and is of the order of the maximum spreading radius of the impinging droplet R_{max} (figure 1(e)); $\dot{L}$ represents the

stretching speed and should be of the order of V_0; $\ddot{L}$ denotes the acceleration rate and scales as V_0^2/R_0; c and k are the damping coefficient and the spring constant, both of which increase with increasing the impact velocity and the PEO concentration [24]; m is the mass of the liquid filament, which can be calculated by $\rho R_{\text{filament}}^2 L$ by assuming the liquid filament takes a cylindrical shape, where $R_{\text{filament}} \approx \sqrt{\rho/c_{\text{PEO}}} R_{\text{fiber}} \approx 9-85 \, \mu\text{m}$ is the filament radius and R_{fiber} being the radius of the residual PEO nanofibers measured from the SEM image (figure S4). Substituting typical values of observed viscoelastic filaments ($R_{\text{max}} \sim O(1.0 \, \text{mm})$, $V_0 \approx 0.1-0.5 \, \text{m s}^{-1}$, $m \sim 10^{-10}-10^{-8} \, \text{kg}$, $c \sim 10^{-4} \text{Ns m}^{-1}$ and $k \sim 1 \text{N m}^{-1}$ [24]), one finds that the viscous and inertial forces are at least 2 orders of magnitude smaller than the elastic force, and thus can be neglected. We further assume that the anchoring sites of viscoelastic filaments on the nanostructured superhydrophobic surface are uniformly distributed, then the total resistance force for the recoiling droplet can be expressed as, $F_{\text{r}} \approx 2\pi n f_{\text{r}} R_{\text{max}}^2 \approx 2\pi n k R_0 R_{\text{max}}^2$, with n being the anchoring site number per unit area. It is noted that increasing the number of polymer chains in the solution or the liquid–solid contact area would cause a larger n and F_{r}. We also point out that the viscous force within the droplet [38, 45], which scales as $\pi \mu R_{\text{max}}^2 V_0/H_{\text{max}}$, is another resisting source of droplet motion, where μ is the dynamic viscosity and H_{max} is the height of the droplet at maximum spreading. However, this term is also much smaller than the elastic force of viscoelastic filaments, and its effects on droplet motion can be ruled out as well. On the other hand, the driving force for droplet recoiling is the capillary force that originates from the impact-induced deformation [46], and it should be proportional to the inertial force of the impinging droplet, i.e. $F_{\text{c}} \propto \rho R_0^2 V_0^2$.

On the superhydrophobic surface at 25°C, an impinging droplet is slightly deformed in the spreading stage ($R_{\text{max}} \sim R_0$) at low impact velocity, and it only touches the top of microscopic surface structures during the whole impact process (i.e., it keeps an ideal Cassie state and n is almost a constant) [13, 24]. Therefore, balancing F_{r} with F_{c} yields the lower threshold velocity for rebound

$$V_{\text{L}} \sim \sqrt{\frac{2\pi n k R_0}{\rho}}. \tag{1}$$

Based on the above equation, one can find that an increase in PEO concentration leads to a larger n and k, and thus a higher V_{L}, agreeing well with the experimental data in figure 2. With the increase of the impact velocity, droplet deformation becomes significant, resulting in a larger spreading extent ($R_{\text{max}} > R_0$). Meanwhile, the liquid would impale into the microscopic surface structures if the wetting pressures exceed the anti-wetting pressure [10, 12, 13]. The wetting pressures are the liquid hammer pressure $P_{\text{H}} \approx 0.2\rho C V_0$ [47, 48], which lasts only a few microseconds on a square-micrometer-sized region around the liquid–solid contact point, and a dynamic pressure $P_{\text{D}} \approx 0.5\rho V_0^2$ [10, 13], which exerts on the droplet–surface contact area for the whole spreading process, where C is the sound speed in the liquid. Although the duration of the liquid hammer pressure is much shorter than the dynamic pressure, it has been demonstrated to play a dominant role for the transition from complete rebound to sticky state during the impact of liquid droplets on structured superhydrophobic surfaces [13, 49–51]. The anti-wetting pressures are the capillary pressures caused by the microprotrusions $P_{\text{CM}} = -2\sqrt{2}\gamma \cos \theta_{a-f}/S_{\text{M}}$ and nanoprotrusions $P_{\text{CN}} = -2\sqrt{2}\gamma \cos \theta_{a-f}/S_{\text{N}}$ with θ_{a-f} being the advancing contact angle on the flat surface and S_i being the distance between two neighboring protrusions. By comparing these terms, we found that the impalement occurs on microprotrusions at $V_0 \gtrsim 0.02 \, \text{m s}^{-1}$ ($S_{\text{M}} \sim 10 \, \mu\text{m}$, $\theta_{a-f} \approx 110°$, $C \approx 1495 \, \text{m s}^{-1}$) and on nanoprotrusions at $V_0 \gtrsim 0.40 \, \text{m s}^{-1}$ ($S_{\text{N}} \sim 500 \, \text{nm}$, figure S1), which enlarges the liquid–solid contact area, and thereby the number of filament anchoring sites n. As a result, the droplet rebound is inhibited above an upper threshold velocity V_{U} of 0.45–0.52 m s^{-1} (figure 2), which is slightly higher than the impalement velocity on nanoprotrusions, and V_{U} increases with increasing c_{PEO}.

We want to point out that when an impinging droplet approaches the target surface, the compression of the air between them would lead to the buildup of a large lubrication pressure, which deforms the droplet bottom into a dimple shape [46]. As a consequence, an air layer is always entrapped below the impinging droplet after contact with the surface, and it subsequently contrasts into an air bubble under the action of surface tension. Although surface roughness affects the initial contact between the droplet and surface [36], the shapes of the finally entrapped bubbles are barely influenced [52]. The entrapment of the air bubble has been theoretically investigated by Mandre *et al* [53], and experimentally resolved in finer details by van der Veen *et al* [54], and Li and Thoroddsen [55] on flat hydrophilic surfaces, and by van der Veen *et al* [52] and Langley *et al* [36] on structured superhydrophobic surfaces. The maximum pressure during the bubble formation $P_{\text{max}} = 0.88 \frac{R_0 V_0^7 \rho^4 \text{Ca}^{1/3}}{P_{0\mu_a} R_0^{1/2} \text{St}^{7/9}}$ [56] serves as another anti-wetting pressure to prevent the liquid impalement, where $\text{Ca} = \mu_a V_0/\gamma$ is the capillary number with μ_a being the viscosity of air, and $\text{St} = \mu_a/\rho V_0 R_0$ is the Stokes number. However, P_{max} ($\sim 3.0 \times 10^9$ Pa) at the upper threshold velocity for

rebound is 7 orders of magnitude higher than P_D (~ 101–135 Pa) and 4 orders of magnitude higher than P_H (~ 1.4–1.6×10^5 Pa). This suggests that the entrapped air bubble would stay below the impinging droplet during the whole impact process, separating the liquid from the surface in a small region near the impact point (which has been experimentally observed in previous studies [36, 52, 56, 57]), and the liquid impalement (either in microprotrusions or in nanoprotrusions) triggered by the hammer pressure should occur at the rim of the entrapped bubble. Indeed, it was found that the residual PEO nanofibers after impact in figure 1(d) highly accumulate at a distance of ~ 50 μm from the impact point, which is in the same order of magnitude with the bubble size $L_b \sim R_0 St^{4/9} \sim 10$ μm [58, 59], indirectly confirming the above analyses.

For impinging droplets on superhydrophobic surfaces at higher temperatures, local heat transfer happens at the solid–liquid contact area, and it is described by the heat conduction equation [60], $\frac{\partial T}{\partial t} = \alpha \frac{\partial^2 T}{\partial y^2}$, where t is the time, α is the thermal diffusivity of the liquid and y is the distance of the liquid to the solid surface. As the impact process is radially symmetric, the one-dimensional heat conduction equation is thus employed for the analysis. A non-dimensional analysis of the equation provides a characteristic thermo-diffusion length $L_T = \sqrt{\alpha \tau}$, in which the characteristic time τ should be on the timescale of droplet impact $\sim (\rho R_0^3/\gamma)^{0.5}$ [46]. We found that L_T is about 25 μm ($\alpha = 0.146$–0.164×10^{-6} m^2 s^{-1}, $\tau \approx 3.8$ ms), which is comparable to the filament sizes (9–85 μm, figure S4) of diverse polymer solutions. It causes the fast evaporation of the water in viscoelastic filaments, significantly reducing their tensile strength, and thus they can easily break up during droplet recoiling (figures 1(a)–(c)). Consequently, a decrease of V_L but an increase of V_U with increasing T was identified in the experiments, regardless of the PEO concentration of impinging droplets (figure 2).

3.2. Contact time

Among diverse characteristics of bouncing droplets, the contact time t_c (i.e. the residence time of an impinging droplet after contact and before taking off the surface [61]) is a key parameter inferring the droplet–surface interaction during impact [17, 46]. For low-viscosity Newtonian liquids such as water, t_c would increase at an impact velocity lower than a critical value, above which it approaches an asymptotic value of $\tau_c \approx 2.6 \left(\frac{\rho R_0^3}{\gamma} \right)^{0.5}$ [24, 61–63]. In figure 3, we comparatively show the contact time of bouncing droplets of 0.1 gl^{-1} and 1.0 gl^{-1} PEO solutions on superhydrophobic surfaces at three different surface temperatures. Evidently, t_c of the same liquid droplets is shorter on hot surfaces than that on cold surfaces at similar impact velocities. By comparison, on superhydrophobic surfaces of same temperature, droplets of high PEO concentrations stay longer than droplets of low PEO concentrations before rebound (figure 3 and figure S5). Similar to low-viscosity Newtonian droplets [43, 63], t_c of aqueous PEO droplets was found to increase with decreasing V_0 at low impact velocities, and this trend stops at a critical velocity (~ 0.27 m s^{-1}), which is close to that of pure water droplets (~ 0.26 m s^{-1}) [24, 49]. However, at higher velocities, t_c first starts to gradually increase (from a value close to τ_c, figure 3) with V_0, and then an obvious increase is observed at $V_0 \gtrsim 0.35$ m s^{-1}, which corresponds to the impalement velocity of liquids into the nanoprotrusions of the superhydrophobic surfaces. By decomposing the impact process into the spreading and retraction stages, one can clearly see that the spreading time (t_s) continuously decreases with the increase of V_0 and the experimental data can still be well described by an empirical power-law for Newtonian droplets [38], $t_s/(\rho R_{max}^3/\gamma)^{0.5} = \xi We^\beta$, while the retraction time t_r shows a similar dependence on V_0, T and c_{PEO} as t_c, where ξ is a coefficient and β is the exponent. This finding further demonstrates that the effects of surface heating on bouncing viscoelastic droplets occur in the retraction stage as a consequence of the reduced droplet–surface interaction.

3.3. Restitution coefficient

To quantitatively characterize the rebound phenomena, we have measured the restitution coefficient ε—another parameter reflecting the droplet–surface interaction in the dynamic conditions [11, 49, 64], and results of those two solutions in figure 3 are plotted in figure 4. Due to their nonspherical shapes (figures 1(a)–(c)), we traced the motion of the center of gravity of impinging droplets, and the restitution coefficient is defined as the ratio of the gravitational potential energy at the highest point of rebound and initial kinetic energy, i.e. $\varepsilon = 2gh_{max}/V_0^2$, where g is the gravitational acceleration and h_{max} is the height of the droplet gravity center with respect to the superhydrophobic surface. Obviously, ε is much smaller than 1 and decreases with increasing V_0 or We for all bouncing droplets, implying strong energy dissipation during impact. The maximum restitution coefficient, which is found at the lower threshold velocity for rebound, decreases from ~ 0.3 for 0.1 gl^{-1} PEO solution to ~ 0.15 for 1.0 gl^{-1} PEO solution on superhydrophobic surfaces at 25 °C (figure 4 and figure S6). However, by increasing surface temperature, ε becomes larger for each aqueous PEO solution and a value up to ~ 0.7 is observed for 0.1 gl^{-1} PEO solution at 95 °C. Most
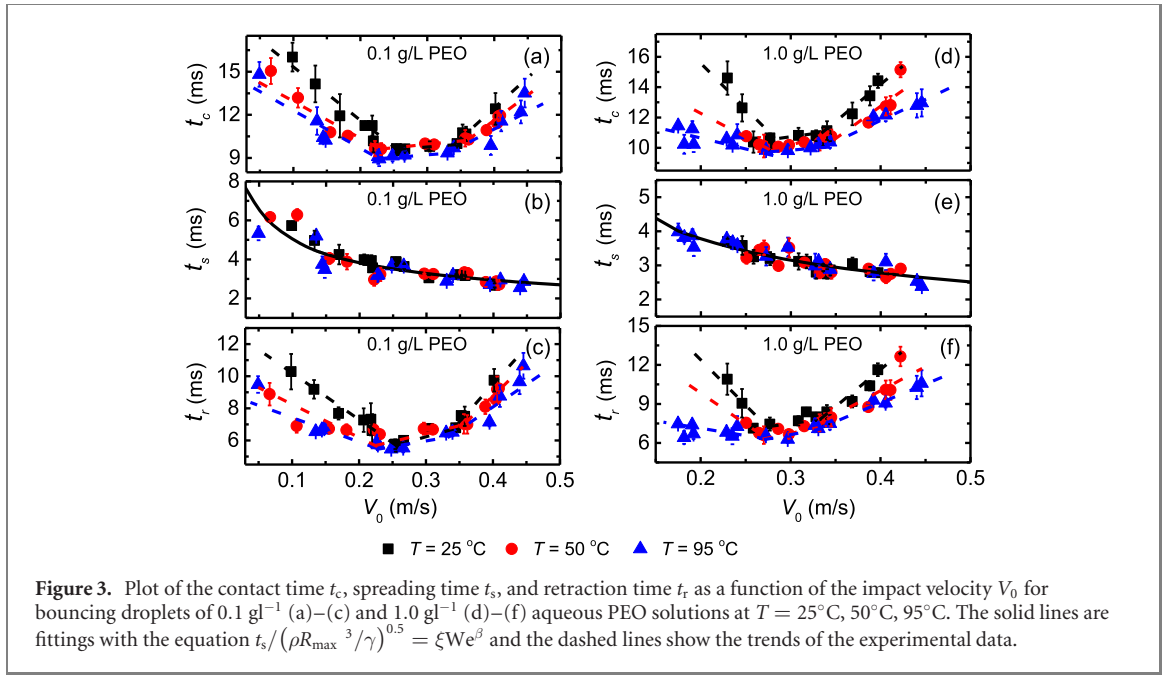
Figure 3. Plot of the contact time t_c, spreading time t_s, and retraction time t_r as a function of the impact velocity V_0 for bouncing droplets of 0.1 gl^{-1} (a)–(c) and 1.0 gl^{-1} (d)–(f) aqueous PEO solutions at $T = 25°C$, $50°C$, $95°C$. The solid lines are fittings with the equation $t_s/\left(\rho R_{max}{}^3/\gamma\right)^{0.5} = \xi We^\beta$ and the dashed lines show the trends of the experimental data.
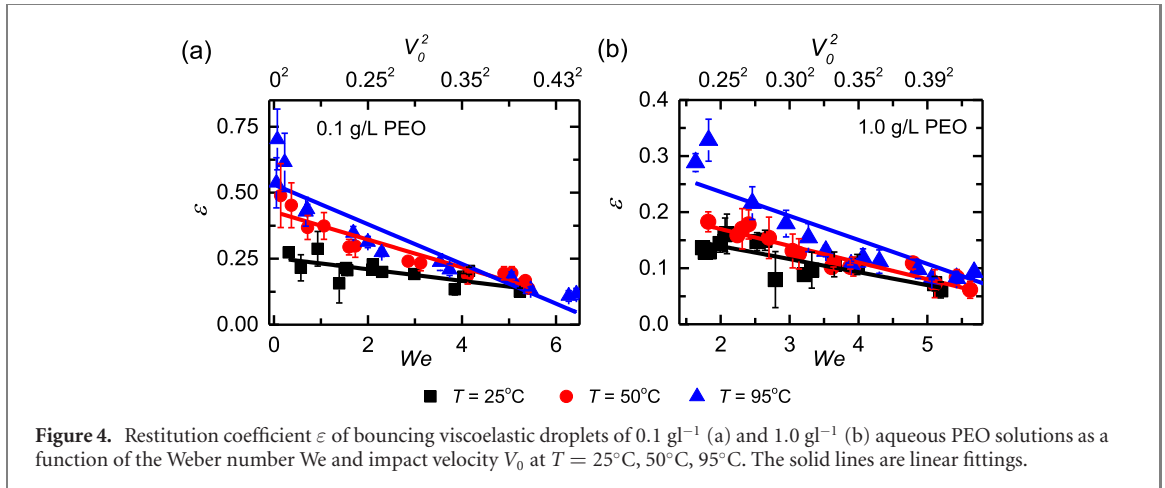
Figure 4. Restitution coefficient ε of bouncing viscoelastic droplets of 0.1 gl^{-1} (a) and 1.0 gl^{-1} (b) aqueous PEO solutions as a function of the Weber number We and impact velocity V_0 at $T = 25°C$, $50°C$, $95°C$. The solid lines are linear fittings.

importantly, we found that the correlation between ε and We can be fitted by a linear function, $\varepsilon = A - B$We, with A and B being two coefficients. The linear behavior is more pronounced for impinging droplets on superhydrophobic surfaces at $T \lesssim 50°C$ and for impinging droplet at We $\gtrsim 2.0$ on superhydrophobic surfaces at $T = 95°C$, regardless of the PEO concentration.

We elucidate the inversely linear dependency of ε on We using a simple scaling argument. As discussed above, the main source dissipating the kinetic energy (E_k) of the impinging droplet is the viscoelastic resistance of the formed filaments, and the dissipated energy scales as $E_{V-E} = \iint df_r\, dL \approx \iint_0^{R_{max}} 2\pi nk R_c L dr\, dL \approx 0.5\pi nk R_{max}^4$. Since the region over which the liquid hammer pressure applied is much smaller than that of the dynamic pressure, n is thus mainly determined by the wetting of surface microprotrusions under P_D. Making reasonable assumptions that these surface microprotrusions are constructed by columns of nanoparticles and the impalement depth of liquid into the microprotrusions increases with the dynamic pressure, one finds that the actual solid–liquid contact area [65] and thus the anchoring sites of viscoelastic filaments should be positively proportional to the Weber number, i.e. $n \propto$ We. Combining these correlations with the spreading law of impinging droplets on non-wetting surfaces, $R_{max} \propto R_0 We^{0.25}$ [46], we obtain $E_{V-E} \propto k R_0^4 We^2$, and the restitution coefficient can be expressed as

$$\varepsilon \approx \frac{E_k - E_{V-E}}{E_k} \propto -\text{We}. \tag{2}$$

It is noted that droplet rebound only happens in an impact event that the input kinetic energy overweights the viscoelastic dissipation energy in the dynamic process. Therefore, the restitution coefficient would take a general form of $\varepsilon = A - B$We as found in the experimental study for impinging droplets at
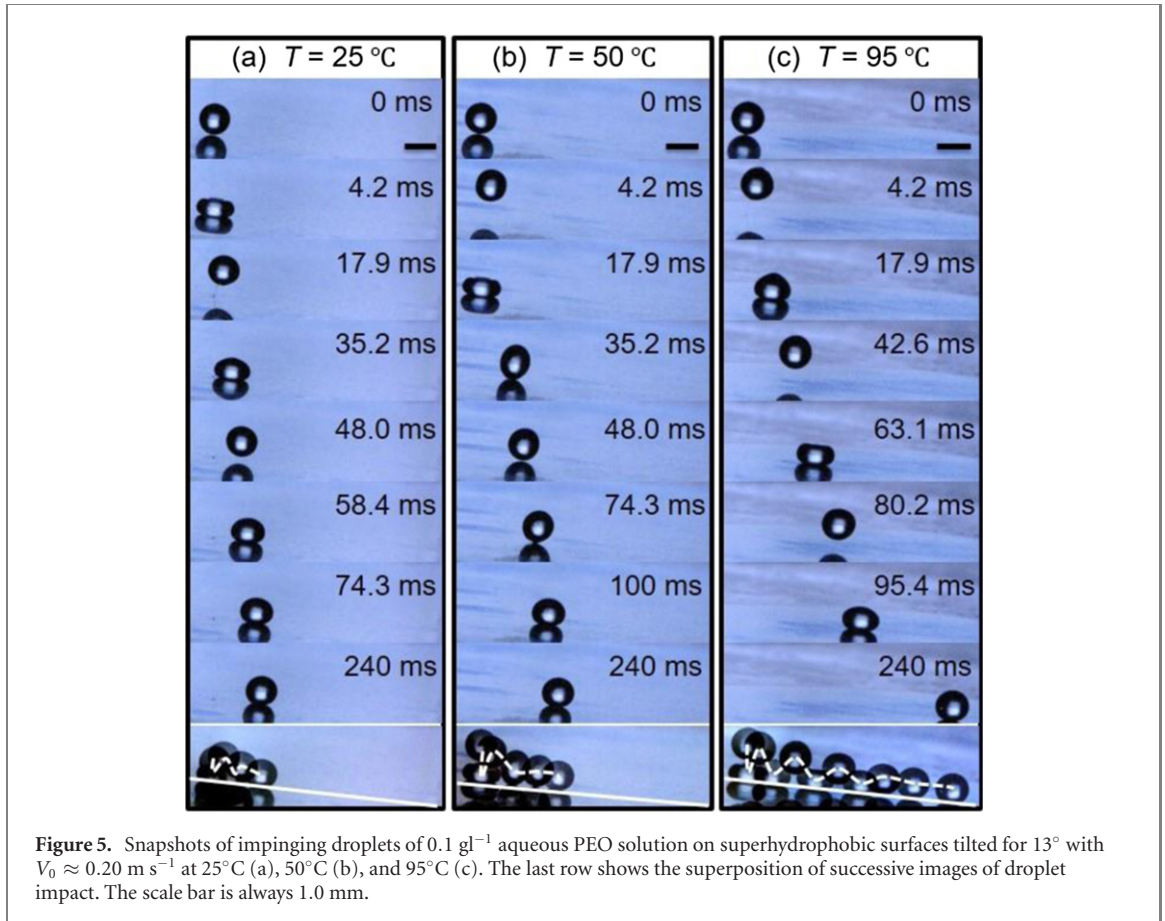
Figure 5. Snapshots of impinging droplets of 0.1 gl^{-1} aqueous PEO solution on superhydrophobic surfaces tilted for 13° with $V_0 \approx 0.20$ m s^{-1} at 25°C (a), 50°C (b), and 95°C (c). The last row shows the superposition of successive images of droplet impact. The scale bar is always 1.0 mm.

$T \lesssim 50°C$. At surface temperature of 95°C, the formed viscoelastic filaments quickly break up during recoiling, which significantly lessens the resistance force and thus leads to a high ε. As such, the linear fitting of the experimental data is compromised, especially for impinging droplets at We $\lesssim 2.0$.

3.4. Droplet deposition after impact on inclined superhydrophobic surfaces

The promoted rebound of impinging droplets will reduce liquid retention on solid surfaces, and thus affect technological processes associated with droplet impact, e.g. pesticide deposition in agricultural spray [15, 16] and heat transfer in spray cooling [66]. To illustrate the influence of surface temperature on the deposition of aqueous PEO solutions on superhydrophobic surfaces, we further performed oblique droplet impact experiments, which are more commonly encountered in real-world applications [17, 46]. As displayed in figure 5(a) and supplemental movie S4, an impinging droplet of 0.1 gl^{-1} PEO solution with $V_0 \approx 0.20$ m s^{-1} rebounds two times on the inclined superhydrophobic surface (with tilting angle of $\sim 13°$) at 25°C, and it gets stuck on the surface at ~ 3 mm away from the impact point. Although only two times of droplet rebounds were observed on the surface at 50°C, the droplet is moved ~ 5 mm due to its larger restitution coefficient (figure 4(a)) and then starts to roll down rather than stops moving (figure 5(b) and supplemental movie S5). In comparison, the number of droplet rebounds is increased to four times on the superhydrophobic surface at 95°C, and the corresponding displacement distance along the surface is ~ 12 mm (figure 5(c) and supplemental movie S6). Similar droplet behaviors were also found for other aqueous PEO solutions. These phenomena indicate an enhancement of the mobility of viscoelastic droplets on superhydrophobic surfaces by surface heating, which would reduce liquid deposition efficiency.

4. Conclusion

In summary, we experimentally investigated the impact dynamics of diverse viscoelastic droplets of aqueous PEO solutions on superhydrophobic surfaces at different temperatures. It was found that increasing surface temperature does not affect the spreading of impinging viscoelastic droplets, but can speed up droplet recoiling and thus promote the rebound behavior. This phenomenon is attributed to the evaporation and breakup of the formed viscoelastic filaments on the heated superhydrophobic surface, which hinder droplet retraction. As a result, the lower threshold velocity, above which droplet rebound occurs, is found to

decrease with increasing surface temperature, while the upper threshold, above which liquid wets the microscopic surface structures and the rebound is inhibited, shows an increase trend with the surface temperature. The contact time is longer for impinging droplets with higher PEO concentrations on colder surfaces, and exhibits a non-monotonic dependence on the impact velocity: below a critical value the contact time significantly increases with decreasing the impact velocity, which is similar to Newtonian droplets, whereas above the critical velocity the contact time first gradually increases and then significantly increases due to the enhanced viscoelastic filament formation. We also found that the restitution coefficient of bouncing viscoelastic droplets linearly decreases with the Weber number, regardless of the PEO concentration. Simple scaling models exploiting the interfacial force and energy analyses are proposed to explain these results. We further demonstrate that the promoted rebound behavior by surface heating can reduce the deposition efficiency of viscoelastic liquids on inclined superhydrophobic surfaces.

Acknowledgments

ORCID iDs

Sang W Joo ● https://orcid.org/0000-0001-9102-4224
Longquan Chen ● https://orcid.org/0000-0002-6785-5914

Reference

[1] Forbes D W J C 1992 *Plants in Agriculture* (Cambridge: Cambridge University Press)
[2] Bixler G D and Bhushan B 2014 Rice- and butterfly-wing effect inspired self-cleaning and low drag micro/nanopatterned surfaces in water, oil, and air flow *Nanoscale* **6** 76–96
[3] Neinhuis C and Barthlott W 1997 Characterization and distribution of water-repellent, self-cleaning plant surfaces *Ann. Bot.* **79** 667–77
[4] Watson G S, Myhra S, Cribb B W and Watson J A 2008 Putative functions and functlona efficiency of ordered cuticular nanoarrays on insect wings *Biophys. J.* **94** 3352–60
[5] Srinivasan S, Chhatre S S, Guardado J O, Park K C, Parker A R, Rubner M F, McKinley G H and Cohen R E 2014 Quantification of feather structure, wettability and resistance to liquid penetration *J. R. Soc. Interface* **11** 11
[6] Baxter A B D C 1945 Large contact angles of plant and animal surfaces *Nature* **155** 21
[7] Quéré D 2008 Wetting and roughness *Annu. Rev. Mater. Res.* **38** 71–99
[8] Cassie A B D and Baxter S 1944 Wettability of porous surfaces *Trans. Faraday Soc.* **40** 546
[9] Simpson J T, Hunter S R and Aytug T 2015 Superhydrophobic materials and coatings: a review *Rep. Prog. Phys.* **78** 086501
[10] Bartolo D, Bouamrirene F, Verneuil É, Buguin A, Silberzan P and Moulinet S 2006 Bouncing or sticky droplets: impalement transitions on superhydrophobic micropatterned surfaces *Europhys. Lett.* **74** 299–305
[11] Richard D and Quéré D 2000 Bouncing water drops *Europhys. Lett.* **50** 769–75
[12] Reyssat M, Pépin A, Marty F, Chen Y and Quéré D 2006 Bouncing transitions on microtextured materials *Europhys. Lett.* **74** 306–12
[13] Deng T, Varanasi K K, Hsu M, Bhate N, Keimel C, Stein J and Blohm M 2009 Nonwetting of impinging droplets on textured surfaces *Appl. Phys. Lett.* **94** 3
[14] Wenzel R N 1936 Resistance of solid surfaces to wetting by water *Ind. Eng. Chem.* **28** 998
[15] Wirth W, Storp S and Jacobsen W 1991 Mechanisms controlling leaf retention of agricultural spray solutions *Pestic. Sci.* **33** 411–20
[16] Hewitt A J 1997 Droplet size and agricultural spraying. 1. Atomization, spray transport, deposition, drift, and droplet size measurement techniques *At. Spring* **7** 235–44
[17] Yarin A L 2006 Drop impact dynamics: splashing, spreading, receding, bouncing *Annu. Rev. Fluid Mech.* **38** 159–92
[18] Bertola V 2013 Dynamic wetting of dilute polymer solutions: the case of impacting droplets *Adv. Colloid Interface Sci.* **193–194** 1–11
[19] Bergeron V, Bonn D, Martin J Y and Vovelle L 2000 Controlling droplet deposition with polymer additives *Nature* **405** 772–5
[20] Bartolo D, Boudaoud A, Narcy G and Bonn D 2007 Dynamics of non-Newtonian droplets *Phys. Rev. Lett.* **99** 4
[21] Zang D, Wang X, Geng X, Zhang Y and Chen Y 2013 Impact dynamics of droplets with silica nanoparticles and polymer additives *Soft Matter* **9** 394–400
[22] Zang D Y, Zhang W X, Song J Y, Chen Z, Zhang Y J, Geng X G and Chen F 2014 Rejuvenated bouncing of non-Newtonian droplet via nanoparticle enwrapping *Appl. Phys. Lett.* **105** 3
[23] Smith M I and Bertola V 2010 Effect of polymer additives on the wetting of impacting droplets *Phys. Rev. Lett.* **104** 4
[24] Chen L, Wang Y, Peng X, Zhu Q and Zhang K 2018 Impact dynamics of aqueous polymer droplets on superhydrophobic surfaces *Macromolecules* **51** 7817–27
[25] Huh H K, Jung S, Seo K W and Lee S J 2014 Role of polymer concentration and molecular weight on the rebounding behaviors of polymer solution droplet impacting on hydrophobic surfaces *Microfluid. Nanofluid* **18** 1221–32

[26] Louhichi A, Charles C-A, Phou T, Vlassopoulos D, Ramos L and Ligoure C 2020 Biaxial extensional viscous dissipation in sheets expansion formed by impact of drops of Newtonian and non-Newtonian fluids *Phys. Rev. Fluids* **5** 053602

[27] Finotello G, De S, Vrouwenvelder J C R, Padding J T, Buist K A, Jongsma A, Innings F and Kuipers J A M 2018 Experimental investigation of non-Newtonian droplet collisions: the role of extensional viscosity *Exp. Fluids* **59** 113

[28] Pack M Y, Yang A, Perazzo A, Qin B and Stone H A 2019 Role of extensional rheology on droplet bouncing *Phys. Rev. Fluids* **4** 123603

[29] Ravikumar S V, Jha J M, Tiara A M, Pal S K and Chakraborty S 2014 Experimental investigation of air-atomized spray with aqueous polymer additive for high heat flux applications *Int. J. Heat Mass Transfer* **72** 362–77

[30] Chen S and Bertola V 2016 The impact of viscoplastic drops on a heated surface in the Leidenfrost regime *Soft Matter* **12** 7624

[31] Bertola V 2009 An experimental study of bouncing Leidenfrost drops: comparison between Newtonian and viscoelastic liquids *Int. J. Heat Mass Transfer* **52** 1786

[32] Bertola V and Sefiane K 2005 Controlling secondary atomization during drop impact on hot surfaces by polymer additives *Phys. Fluids* **17** 108104

[33] Osio J B and Bertola V 2011 Dynamics of viscoelastic drops impacting on heated surfaces in the Leidenfrost regime *24th European Conf. on Liquid Atomization and Spray Systems*

[34] Bertola V 2014 Effect of polymer concentration on the dynamics of dilute polymer solution drops impacting on heated surfaces in the Leidenfrost regime *Exp. Therm. Fluid Sci.* **52** 259–69

[35] Pham J, Paven M, Wooh S, Kajiya T, Butt H-J and doris v 2017 Spontaneous jumping, bouncing and trampolining of hydrogel drops on a heated plate *Nat. Commun.* **8** 905

[36] Langley K R, Li E Q, Vakarelski I U and Thoroddsen S T 2018 The air entrapment under a drop impacting on a nano-rough surface *Soft Matter* **14** 7586–96

[37] Quéré D 2013 Leidenfrost dynamics *Annu. Rev. Fluid Mech.* **45** 197–215

[38] Guo J W, Lin S J, Zhao B Y, Deng X and Chen L Q 2018 Spreading of impinging droplets on nanostructured superhydrophobic surfaces *Appl. Phys. Lett.* **113** 5

[39] Renardy Y *et al* 2003 Pyramidal and toroidal water drops after impact on a solid surface *J. Fluid Mech.* **484** 69–83

[40] Chen L, Li L, Li Z and Zhang K 2017 Submillimeter-sized bubble entrapment and high-speed jet during droplet impact on solid surfaces *Langmuir* **33** 7225

[41] Bartolo D, Josserand C and Bonn D 2006 Singular jets and bubbles in drop impact *Phys. Rev. Lett.* **96** 124501

[42] Chen L, Wu J, Li Z and Yao S 2011 Evolution of entrapped air under bouncing droplets on viscoelastic surfaces *Colloids Surf.* A **384** 726–32

[43] Chen L Q and Li Z G 2010 Bouncing droplets on nonsuperhydrophobic surfaces *Phys. Rev.* E **82** 016308

[44] Ward I M 2012 *Mechanical Properties of Solid Polymers* (New York: Interscience (Wiley-Interscience))

[45] Fedorchenko A I, Wang A B and Wang Y H 2005 Effect of capillary and viscous forces on spreading of a liquid drop impinging on a solid surface *Phys. Fluids* **17** 8

[46] Josserand C and Thoroddsen S T 2016 Drop impact on a solid surface *Annu. Rev. Fluid Mech.* **48** 365–91

[47] Bowden F P and Brunton J H 1961 The deformation of solids by liquid impact at supersonic speeds *Proc. R. Soc.* **263** 433–50

[48] Cook S S 1928 Erosion by water-hammer *Proc. R. Soc.* **119** 481

[49] Chen L, Xiao Z, Chan P C H, Lee Y-K and Li Z 2011 A comparative study of droplet impact dynamics on a dual-scaled superhydrophobic surface and lotus leaf *Appl. Surf. Sci.* **257** 8857–63

[50] Dash S, Alt M T and Garimella S V 2012 Hybrid surface design for robust superhydrophobicity *Langmuir* **28** 9606–15

[51] McCarthy M, Gerasopoulos K, Enright R, Culver J, Ghodssi R and Wang E 2012 Biotemplated hierarchical surfaces and the role of dual length scales on the repellency of impacting droplets *Appl. Phys. Lett.* **100** 263701

[52] van der Veen R, Hendrix M, Tran T, Sun C, Tsai P and Lohse D 2014 How microstructures affect air film dynamics prior to drop impact *Soft Matter* **10** 3703

[53] Mandre S, Mani M and Brenner M P 2009 Precursors to splashing of liquid droplets on a solid surface *Phys. Rev. Lett.* **102** 134502

[54] van der Veen R C A, Tran T, Lohse D and Sun C 2012 Direct measurements of air layer profiles under impacting droplets using high-speed color interferometry *Phys. Rev.* E **85** 026315

[55] Li E Q and Thoroddsen S T 2015 Time-resolved imaging of a compressible air disc under a drop impacting on a solid surface *J. Fluid Mech.* **780** 636–48

[56] Maitra T, Tiwari M K, Antonini C, Schoch P, Jung S, Eberle P and Poulikakos D 2013 On the nanoengineering of superhydrophobic and impalement resistant surface textures below the freezing temperature *Nano Lett.* **14** 1106

[57] Maitra T, Antonini C, Tiwari M K, Mularczyk A, Imeri Z, Schoch P and Poulikakos D 2014 Supercooled water drops impacting superhydrophobic textures *Langmuir* **30** 10855–61

[58] Bouwhuis W *et al* 2012 Maximal air bubble entrainment at liquid-drop impact *Phys. Rev. Lett.* **109** 264501

[59] Hendrix M H W, Bouwhuis W, van der Meer D, Lohse D and Snoeijer J H 2016 Universal mechanism for air entrainment during liquid impact *J. Fluid Mech.* **789** 708–25

[60] Carslaw H S and Jaeger J C 1959 *Conduction of Heat in Solids* 2nd edn (Oxford: Oxford University Press)

[61] Richard D, Clanet C and Quéré D 2002 Surface phenomena—contact time of a bouncing drop *Nature* **417** 811

[62] Biance A-L, Chevy F, Clanet C, Lagubeau G and Quéré D 2006 On the elasticity of an inertial liquid shock *J. Fluid Mech.* **554** 47–66

[63] Okumura K, Chevy F, Richard D, Quéré D and Clanet C 2003 Water spring: a model for bouncing drops *Europhys. Lett.* **62** 237–43

[64] Mouterde T, Lecointre P, Lehoucq G, Checco A, Clanet C and Quéré D 2019 Two recipes for repelling hot water *Nat. Commun.* **10** 1410

[65] Sun Q *et al* 2019 Surface charge printing for programmed droplet transport *Nat. Mater.* **18** 936–41

[66] Pasandideh-Fard M, Aziz S D, Chandra S and Mostaghimi J 2001 Cooling effectiveness of a water drop impinging on a hot surface I *Int. J. Heat Fluid Flow* **22** 201–10